5.0 DATA

The data used to test the hypothesis and aims introduced in the previous chapter are drawn from a set of simulated rs-fMRI sequences and four clinical groups. In this chapter, we will first discuss the mechanism built to simulate brain activity, scanner noise, and motion in rs-fMRI sequences. Then we will discuss the clinical images, which were taken from two studies: a prospective study of congenital heart defects in pediatric patients and a prospective study of Alzheimer's disease in the aging population. Subjects from these two studies were chosen because patient motion causes problems in MR images across all stages of life, though patients may exhibit different types of motion at different stages of life.

5.1 SIMULATED SEQUENCES

There are two major barriers in medical imaging research. The first barrier is that it is difficult to obtain enough data from a large number of subjects to perform large-scale studies. The second barrier is the complexity of identifying a gold standard. Specifically, if the gold standard brain signal which motion correction techniques attempt to recover was known, there would be no need for image processing in the first place. We addressed these two barriers by creating a mechanism for generating a simulated image sequence which includes functional connectivity based brain activity, scanner noise, and simulated patient motion. Our mechanism can create large quantities of unique image sequences. The simulated image sequences can also serve as a gold standard for evaluating volume registration and motion correction techniques: the signals and noise sources added to the sequence are known with certainty.

5.1.1 SPECTr: Simulated Phantom Emulating Cranial Transformations

Our mechanism is called Simulated Phantom Emulating Cranial Transformations (SPECTr). A phantom is an object designed to have material properties which mimic those of a specific tissue type or organ. Phantoms, either manufactured or healthy human, are used in multi-center studies to obtain images of the same object or person from multiple scanners. These images are used to harmonize the data taken from the different sites. We call our simulated sequence a phantom because the baseline image itself is known as are the signals added to it to simulate brain activity and cranial motion.

The process for generating a simulated sequence using SPECTr has several steps and uses a known rs-fMRI sequence. First, a single image volume is selected from the known rs-fMRI sequence. A mask of this volume is created and will be used later in the SPECTr pipeline. The chosen volume is duplicated to create a sequence with N (default $N = 150$) instances of the same volume. This sequence is called the base phantom sequence.

Next, brain signal is added to the base phantom sequence. The location of the brain signals is limited to locations associated with the default mode network (CITATION). Information about healthy default mode networks are used to inform how much simulated BOLD signal could occur in different brain locations over time. In areas associated with healthy default mode networks, small signals are added. These signals are mixtures of 3D Gaussian distributions. Each distribution's standard deviation and intensity scaling factor change between image volumes. These simulated BOLD signals are saved in a standalone simulated BOLD signal image file. They are also added to the base phantom sequence to create our BOLD phantom sequence. The BOLD phantom sequence serves as the ground truth for any motion correction pipeline: it contains the known brain orientation and BOLD signal independent from head motion and scanner noise.

Now that the ground truth brain orientation and BOLD signal have been established, patient motion can be added to the BOLD phantom sequence. First, a reasonable range of head rotation about the x-, y-, and z-axes was established. These angle ranges are used to generate rotational transformation matrices for $N - 1$ image volumes. The transformations are applied to each image volume after the first volume in the BOLD phantom sequence. The

transformed image sequence is referred to as the BOLD phantom sequence with motion and the rotational transformation matrices are saved as the ground truth for the transformations between each image volume and the template volume.

Finally, scanner noise is added to the BOLD phantom sequence with motion. As discussed in Chapter 2, there are several sources of scanner noise caused by combinations of electromagnetic signal changes in the magnetic field and tissue susceptibility due to patient motion. These noise sources are not addressed in this work, but are simulated as part of SPECTr's pipeline. SPECTr models scanner noise as a randomly generated speckle pattern which is applied to each volume in the BOLD phantom sequence. The sequence containing simulated BOLD signal, patient motion, and scanner noise can now be used to evaluate the efficacy of motion correction pipelines in removing motion and scanner noise from rs-fMRI sequences.

5.1.2 Simulated Images

We used a healthy adult male rs-fMRI as the known rs-fMRI sequence for SPECTr and created 100 simulated sequences. The parameters for the BOLD signal, the head rotations, and the speckle patterns are as follows:

- **BOLD Signal**
  - Standard deviation range: [1, 5]
  - Signal scaling range: [1, 5]
- **Head Rotations (Patient Motion)**
  - Rotation about z-axis (looking left and right): $[-75°, 75°]$ assuming looking left is a negative rotation and looking straight forward is $0°$
  - Rotation about y-axis (looking up and down): $[45°, -20°]$ assuming looking down is a negative rotation and looking straight forward is $0°$
  - Rotation about the x-axis (stretching neck by bringing left ear to left shoulder or right ear to right shoulder): $[-60°, 60°]$ assuming leaning right is a negative rotation and looking straight forward is $0°$
- **Speckle Patterns (EM Scanner Noise)**

– Speckle variance: variance of the uniform distribution used to generate the speckle noise, uses the range [0.05, 1]

The source code for SPECTr is available on Github.

5.1.3 Purpose of Dataset

The phantom experiments are used to probe the volume registration techniques and the motion correction technique. By applying the DAG-based and traditional registration techniques to the base phantom sequence, we evaluate the degrees of positional and signal change errors each technique may introduce into the registration process. The registered versions of the BOLD phantom sequence are compared to each other and to the original BOLD phantom sequence to determine how well each registration retains the BOLD signal.

This particular experiment will be one of the first to investigate how much true BOLD signal is preserved through motion correction. One of the major drawbacks to existing motion correction pipelines is that they remove signal along with noise. In clinical data, there is no way to know the ground truth signal contained within the image; however, simulated phantom images have a de facto known ground truth signal. The design for this experiment can be used to evaluate how much BOLD signal is recovered by other motion correction pipelines, and how close the recovered signal is to the signal of interest.

5.2 CONGENITAL HEART DISEASE COHORTS

Congenital heart defects and congenital heart disease (CHD) both refer to defects in the heart or the vessels around the heart which formed during fetal development. Heart defects affect how blood moves into, through, and away from the heart. However, cardiac conditions are not the only complications CHD must deal with. In recent years, researchers have found that there is a relationship between CHD and neurocognitive disorders. The CHD rs-fMRIs used in this study were gathered as part of ongoing studies of the relationship between CHD and neurodevelopment. Data from these studies was obtained through studies approved by

the IRB at the Children's Hospital of Pittsburgh of UPMC and the University of Pittsburgh. The data is stored and accessed in compliance with all HIPPA policies.

5.2.1 CHD and Neurodevelopment

CHD consists of a variety of defects affect the vessels and chambers of the heart. It has a worldwide prevalence of about 8 per 1000 live births, meaning about 1.35 million children are born with CHD every year. Since the survivability of CHD has increased from 10% to 90%, the medical community is faced with a growing, aging population of CHD patients. Many of these patients also suffer from neurocognitive disorders that co-occur with CHD. The neurocognitive disorders are usually diagnosed using at least one of many psychological survey-based evaluations, but these methods are subjective. rs-fMRIs could be used to identify patients who have functional connectivity patterns associated with different neurocognitive disorders, and eventually may be used to identify patients who are at risk for developing these disorders.

CHD can affect any combination of heart chambers and blood vessels with varying degrees of severity. The lesions prevent the cardiopulmonary system as a whole from functioning correctly, but pinpointing and treating the defects effectively can be a complex process.

There are a number of genetic and environmental factors associated with different presentations of CHD [Mozaffarian et al., 2016]. Genetic conditions such as Down syndrome, Turner syndrome, 22q11 deletion syndrome, Williams syndrome, and Noonan syndrome are associated with different CHD presentations. Maternal behaviors such as smoking and binge drinking are known to cause heart problems in the fetus. Other maternal risk factors are obesity, folate deficiency, and living at a high altitude. Paternal exposure to phthalates, anesthesia, sympathomimetic medications, pesticides, and solvents may increase the risk of the fetus for developing CHD. While there are quite a few factors in this list, there are many CHD cases whose causes are unknown.

The process of diagnosing CHD can begin before birth. A specialized ultrasound test called fetal echocardiography can detect heart abnormalities as early as the second trimester of the pregnancy. Additional tests, such as amniocentesis and follow-up ultrasounds may be

Table 15-3. Estimated Prevalence of Congenital Cardiovascular Defects and Percent Distribution by Type, United States, 2002* (in Thousands)

	Prevalence, n			Percent of Total		
Type	Total	Children	Adults	Total	Children	Adults
Total	994	463	526	100	100	100
VSD†	199	93	106	20.1	20.1	20.1
ASD	187	78	109	18.8	16.8	20.6
Patent ductus arteriosus	144	58	86	14.2	12.4	16.3
Valvular pulmonic stenosis	134	58	76	13.5	12.6	14.4
Coarctation of aorta	76	31	44	7.6	6.8	8.4
Valvular aortic stenosis	54	25	28	5.4	5.5	5.2
TOF	61	32	28	6.1	7	5.4
AV septal defect	31	18	13	3.1	3.9	2.5
TGA	26	17	9	2.6	3.6	1.8
Hypoplastic right heart syndrome	22	12	10	2.2	2.5	1.9
Double-outlet right ventricle	9	9	0	0.9	1.9	0.1
Single ventricle	8	6	2	0.8	1.4	0.3
Anomalous pulmonary venous connection	9	5	3	0.9	1.2	0.6
Truncus arteriosus	9	6	2	0.7	1.3	0.5
HLHS	3	3	0	0.3	0.7	0
Other	22	12	10	2.1	2.6	1.9

Average of the low and high estimates, two thirds from low estimate.[24]ASD indicates atrial septal defect; AV, atrioventricular; HLHS, hypoplastic left heart syndrome; TGA, transposition of the great arteries; TOF, tetralogy of Fallot; and VSD, ventricular septal defect.

*Excludes an estimated 3 million bicuspid aortic valve prevalence (2 million in adults and 1 million in children).

†Small VSD, 117 000 (65 000 adults and 52 000 children); large VSD, 82 000 (41 000 adults and 41 000 children).

Source: Data derived from Hoffman et al.[24]

Figure 10: Table of prevalences of congenital heart defects borrowed temporarily from [Mozaffarian et al., 2016].

used to determine treatment options before the patient is born. Generally, severe CHD cases present and are detected at earlier stages, but minor defects may not become apparent until the patient is older. Tests used to diagnose CHD in postnatal patients include electro- and echo-cardiograms, chest x-rays, pulse oximetry, exercise stress tests, computed tomography or MRI scans, and cardiac catheterization. Treatment of different defects varies from monitoring and medication to surgery and cardiac implants.

The incidence of CHD in live births vary across countries and continents. The United States reports approximately 4-10 CHD case per 1000 live births. Europe and Asia see about 6.9 and 9.3 CHD cases per 1000 live births [Mozaffarian et al., 2016]. In China, the incidence of CHD ranges from 8.98 to 11.1 per 1000 live births [Zhao et al., 2019] [Qu et al., 2016]. A pair of studies from Iran report incidences of 8.6 and 12.3 per 1000 live births, though the studies note that they were performed in different geographical locations with different populations within the country [Nikyar et al., 2011] [Rahim et al., 2008]. One report from Dharan reports an incidence of 5.8 per 1000 patients admitted to a tertiary care hospital

over a 12 month period [Shah et al., 2008]. A study of newborns at one hospital in New Delhi, India claims an incidence of 3.9 per 1000 live births, though this rate may be a poor estimate as there is a significant delay between patient birth and referral to a cardiac center in India [Khalil et al., 1994] [Saxena, 2005].

These incidence rates should be analyzed with some caution. In many cases, the reported rates were based on medical records. Medical records are not always correct. Additionally, the only way for a person to have a medical record is for him to go to a medical center. Not everyone who has CHD is able to seek medical help, often because of their geographical locations or their income. Even if a patient is able to seek medical help, the availability of proper cardiac care varies between and within countries.

As screening tools become more effective and more widespread, it is expected that incidence rates will increase as defects are detected earlier. Generally, the earlier a defect is detected, the earlier it can be treated. Early detection and treatment means more CHD patients will live to adulthood. Currently, Webb et al. estimate that at least 12 to 34 million adults have CHD, and this number is expected to increase [Webb et al., 2015].

It is important to note that each defect type has a different prevalence, a different treatment plan, and different expected outcomes. A breakdown of prevalence rates of some of the most common lesion types can be seen in Figure 10. Once a patient is diagnosed with one of these defects, the specific nature of his case must be clearly documented. The documentation of CHD using the International Classification of Diseases, Ninth Revision, Clinical Modification (ICD-9-CM) has 25 high level codes representing various presentations of CHD, but these codes used alone are often not sufficient for describing a patient's true condition [Mozaffarian et al., 2016]. Additional ICD-9-CM codes should be used to communicate the finer details of a patient's condition.

The financial burden of CHD varies depending on the defect. Certain defects require complex, expensive surgical repairs while others can be treated with less expensive approaches [Mozaffarian et al., 2016]. The burden of CHD across the globe was outlined by Webb et al. Their figure illustrating the prevalence of CHD and the availability of funds with which to treat it can be see in Figure 11. As the overall mortality of CHD declines, the burden of CHD is expected to increase [Mozaffarian et al., 2016].

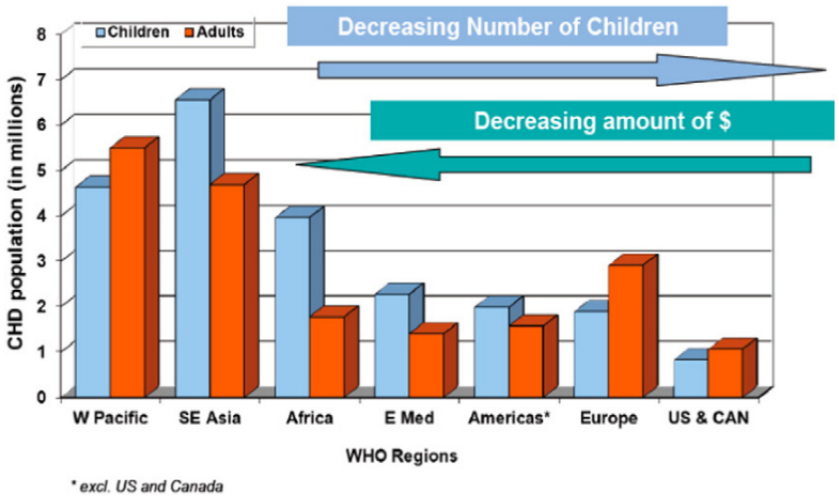

Figure 11: Estimated CHD burden in World Health Organization (WHO) regions using incidence rates of approximately 12/1000 and 4/1000 in children and adults, respectively [Webb et al., 2015].

Unfortunately, the cost of treating CHD alone is not the only burden a patient must undergo. Patients with CHD are also at increased risk for heart failure and infections [Mozaffarian et al., 2016]. Children with CHD are at 19-fold risk for stroke compared to their healthy counterparts [Fox et al., 2015]. In a study of Swedish citizens born between 1970 and 1993, Giang et al performed a study compared the prevalence of cardiac conditions in patients with and without CHD [Giang et al., 2018]. They found that patients who had a CHD diagnosis were at about eight times higher risk for intracerebral hemorrhage and subarachnoid hemorrhage than their non-CHD counterparts. The CHD patients were also more likely to suffer from arrhythmia and heart failure.

5.2.2 Potential Causes of Neurodevelopmental Complications

Early research in this area focuses on the neurodevelopmental status of neonatal patients pre- and post-surgical intervention. One theory was that some factor or factors in the surgical intervention caused brain injuries in the patients. This idea proved to be inaccurate when

researchers began detecting neurological malformations *in utero*.

In a systematic review of available literature regarding prenatal and postnatal presurgical CHD cases and neurodevelopmental outcomes, Mebius et al. identify two theories about the causality of neurodevelopmental delays and CHD [Mebius et al., 2017]. The first theory is that abnormalities in the cardiac system prevent the developing brain from receiving enough oxygen and nutrients, which disrupts prenatal brain development. The second theory is that faulty genetic pathways used during both cardiac and brain development cause both conditions to co-occur. However, 11 articles Mebius et al. found during their review that are related to bloodflow through the umbilical artery suggest a third theory. During the prenatal period, a fetus receives oxygen from the mother via the placenta. If the placenta was not functioning correctly, it could lead to the fetus receiving not enough oxygen. Lower quantities of oxygen throughout prenatal development could potentially cause problems both in brain and cardiac growth. The 11 articles have contradictory results, but some researchers are currently investigating the role of the placenta in CHD and prenatal brain development.

5.2.3 Aging

Survival of CHD patients to adulthood has increased from 10% to 90% over the last several decades. The impact of the combination of CHD and neurological conditions throughout a patient's lifetime is starting to be explored. The aging of the CHD population has also sparked interest in the relationships between CHD and adult-stage neurological disorders such as dementia and Alzheimer's.

5.2.4 Identifying Neurocognitive Disorders

5.2.4.1 Patient Surveys Surveys known to be used for studying the relationship between CHD and neurodevelopment are

- National Institute of Health Toolbox (3 - 85 years): "Performance tests of cognitive, motor, and sensory function and self-reported measures of emotional function for adults and children in the general population and those living with a chronic condition".

- Sue Beers (4 - 18 years [not inclusive of 18 years]): WASI-II, NEPSY-2, WRAML-2, D-KEFS, WISC-IV, Grooved Pegboard, BRIEF, Beery-Buktenica VMI, ASRS, Conners-3, BASC-II, ABAS-II, PedsQL General, PedsQL Cardiac, Pictoral Scale Self Perception Profile.
- SVR-III NDT (9 - 13 years [not inclusive of 13 years]): WIAT, NEPSY, WRAML, D-KEFS, WISC-V, Grooved Pegboard, BRIEF, Beery-Buktenica VMI, ASRS, Conners ADHD Index, BASC-II, ABAS-3, PedsQL General, PedsQL Cardiac
- Bayley Scales of Infant and Toddler Development -III (1 - 24 months): Subtests include cognitive, language, social-emotional, motor, and adaptive behavior tests [Mebius et al., 2017].
- Battelle Developmental Inventory (Birth - 8 years [not inclusive of 8 years]): Subsets include cognition, communication, social-emotional development, physical development, and adaptive behavior.
- Developmental Assessment of Young Children (Birth - 6 years [not inclusive of 6 years]): Subtests include cognition, communication, social-emotional development, physical development, and adaptive behavior.
- Preschool Language Scale + Receptive-Expressive Emergent Language (Birth - 3 years): Total language, auditory comprehension, expressive communication, articulation, receptive language, expressive language, and inventory of vocabulary words.
- Peabody Developmental Motor Scales (Birth - 5 years): Subtests include reflexes, stationary, locomotion, object manipulation, grasping, visual-motor integration

The goal of these surveys is to compare the patient's cognitive function and neurological functions to expected milestones. Certain deviations from certain milestones are indicative of different disorders.

5.2.4.2 Neurological Images When an area of the brain is active, it uses more oxygen than the surrounding regions. Functional MRIs (fMRI) are sensitive to signals emitted by deoxygenated hemoglobin. The blood oxygen level dependent (BOLD) signal recorded by the fMRI reveal regions of the brain which are active at the same time. These combinations of regions are called neuronal networks.

Many neuronal networks exist, but most of them are considered to be task related. In 2001, Raichle et al. suggested the existence of a neuronal network which operated when a person is at rest [Raichle et al., 2001]. Their theory was confirmed by Greicius et al. in 2003 [Greicius et al., 2003]. Because the patient is not performing a specific task when they are in a resting state, the resting-state networks have the potential to reveal valuable information about a patient's neurodevelopmental status.

A fMRI taken of a patient in a resting, task-free state, is called a resting-state fMRI (rs-fMRI). rs-fMRIs are sequences of image volumes acquired over a period of a few minutes. The image volumes themselves have relatively low spatial resolution when compared to structural MRIs, but their temporal resolution is significantly higher as a new volume is acquired every two to three seconds.

The BOLD signals in rs-fMRI image sequences are analyzed using a process called functional connectivity analysis. Functional connectivity analysis identifies patterns and networks of brain activity. Some functional connectivity analysis studies have lead to the discoveries of links between specific disruptions in these naturally occurring networks and neurodevelopmental diseases such as autism and attention deficit hyperactivity disorder [Assaf et al., 2010] [Zang et al., 2007]. With further refinements of both acquisition techniques and characterization of these functional networks, clinicians may be able to use rs-fMRI to evaluate the neurodevelopmental status of CHD patients and to identify patients who may benefit from certain therapies or neuroprotective interventions.

5.2.5 CHD Subjects

5.2.5.1 Neonatal Subject Population and Images Neonatal subjects are recruited as part of a prospective observational study. The subjects were scanned using a 3T Skyra (Siemans AG, Erlangen, Germany). They were unsedated during the scans and a "feed and bundle" protocol was used to prevent motion during the scans [Windram et al., 2011]. The newborns were positioned in the coil to minimize head tilting. Newborns were fitted with earplugs (Quiet Earplugs; Sperian Hearing Protection, San Diego, CA) and neonatal ear muffs (MiniMuffs; Natus, San Carlos, CA). An MR-compatible vital signs monitoring

system (Veris, MEDRAD, Inc. Indianola, PA) was used to monitor neonatal vital signs. All scans were performed using a multi-channel head coil. The parameters for the resting-state BOLD MR scans were FOV=240 mm and TE/TR=32/2020 ms with interplane resolution of 4x4 mm, slice thickness of 4 mm, and 4 mm space between slices. The acquired images contained 150 volumes where each volume consisted of 64x64x32 voxels^3.

5.2.5.2 Preadolescent Subject Population and Images As part of a multicenter study of CHD in preadolescents, we collected rs-fMRIs from nine sites throughout the United States. These images were of patients in the age range of 9 to 13 years who either had CHD or were healthy with no neurocognitive impairments. In addition to the MRI scans, subjects who participated in this study were asked to participate in additional testing either to determine their neurocognitive outcome status or to perform genetic analyses.

5.2.5.3 Fetal Subject Population and Images Fetal subjects have different constraints on their physical environment than neonates, preadolescents, and adults. As a result, they exhibit unique patterns of motion. The previous subject cohorts discussed in this chapter have the following commonalities: the subject experiences the full effects of gravity, the subject is lying on his back in an MRI scanner, and the subject's head motion is limited by the head coil within the MRI. Any motion in these images is a direct result of the subject himself moving, whether passively (cardiac motion and breathing) or actively (fidgeting or looking around).

A fetal subject is scanned in vivo. He is suspended in amniotic fluid within his mother. The amniotic fluid has buoyancy that reduces the effects of gravity and allows a fetal subject significant freedom of movement. The fetus can rotate, shift, and flip in ways that can only be accomplished when floating in a body of water. The properties of the uterus constrain the physical space in which a motion could occur, but not as much as the head coil and gravity do to the other patient cohorts. A fetus is not guaranteed to be in any specific position at the start of the scan: the scan begins when the mother is ready, not when the fetus achieves a certain pose.

The fetal subjects underwent fetal echocardiography scans in a cardiac clinic to determine

whether they were healthy or had a form of CHD. They were then scanned on an MRI scanner. Images of the fetal brain and the placenta were acquired for each subject.

We are interested in both the fetal brain and placental images for our work because of the relationship between placenta and brain development. However, these organs have very different physical properties. The fetal brain is a rigid structure floating and moving within the amneotic fluid. It undergoes translation and rotation as a single unit due to passive and active maternal and fetal motions. The placenta, on the other hand, is anchored in place on the uterine wall. It may undergo small translations or rotations due to maternal motion, but it will respond differently to fetal motion. Fetal motions cause nonlinear deformations of the pliable placenta that can only be adequately accounted for using nonlinear registration algorithms. Nonlinear registrations have the potential to deform brain images into physically impossible shapes, so the fetal brain and placenta were manually segmented in their respective images so that each organ could undergo independent motion correction.

The segmenters were one of a group of four researchers. While one researcher trained the other three group members, the interrater agreement between them is still being determined.

5.2.6 Purpose of Dataset

Neonatal Cohort. Our set of neonatal subjects includes a cohort of 74 healthy neonates. Each subject in this cohort underwent an MRI scan, and the rs-fMRIs obtained during this process were compared to Power et al.'s positional and signal change usability thresholds. Of the 74 subjects, 17 of them had rs-fMRIs which did not meet the usability criteria. These high motion images were used to test the feasibility of the DAG-based volume registration framework.

These images were ideal for the feasibility study for three reasons. First, the neonates were healthy, which eliminates disease status as a confounding variable in the analysis of the registered images. Second, the neonates in this study were scanned using a feed and sleep protocol. Because the neonates were asleep during the scan, they generally did not move very much. The high-motion neonates are an obvious exception to this concept, but many of the high-motion images contained long periods where the subject was stationary.

Evaluating the DAG-based framework on data with various patterns of motion and different periods of low and high motion allowed us to explore the effects of the DAG-based algorithm in different combinations of motion features. Third, these images were too corrupted by motion to be used in other analyses. Applying both the DAG-based framework and the traditional registration framework to these images provided the opportunity to compare the performances of both registration frameworks to each other in the context of the usability gold standard thresholds.

Preadolescent Cohort. The multicenter imaging study of preadolescent subjects provides a unique opportunity to evaluate the efficacy of the DAG-based framework on a large subject cohort containing variable amounts of motion. The outcome of this experiment will be used in the next experiment to determine if there are any site-specific or vendor-specific variables influencing patient motion.

Fetal Cohort. As the fetal subjects have both neurological and placental images, their data will be used to examine the impact of volume registration on different organ types.

5.3 AGING BRAIN SUBJECTS

The final data set we use is from the Alzheimer's Disease Neuroimaging Initiative (ADNI) database (adni.loni.usc.edu). The ADNI was launched in 2003 as a public-private partnership, led by Principal Investigator Michael W. Weiner, MD. The primary goal of ADNI has been to test whether serial magnetic resonance imaging (MRI), positron emission tomography (PET), other biological markers, and clinical and neuropsychological assessment can be combined to measure the progression of mild cognitive impairment (MCI) and early Alzheimer's disease (AD). For up-to-date information, see www.adni-info.org.

5.3.1 Purpose of Dataset

The adult cohort encompass many clinical outcomes and a wider age range than the other clinical populations. The adult cohort also allows for another opportunity to study a different

type of motion patterns associated with the aging brain rather than the still-developing brain.

5.4 SUMMARY

In this chapter, we discussed our three major data sets, which are drawn from simulated data, pediatric data, and aging brain data. The simulated data were generated using a rs-fMRI simulation pipeline developed in-house and were used for the purpose of measuring ground truth signal recovered by motion correction techniques. The pediatric data were obtained through prospective studies of CHD and neurodevelopment being conducted at the UPMC Children's Hospital of Pittsburgh. The aging brain images were downloaded from the ADNI study. The pediatric and aging brain images were used to compare the two volume registration techniques in a standalone analysis as well as in the context of a motion correction pipeline. We also used these images to examine patterns of motion unique to different age groups.